

## Dynamics of Charged Excitons and Biexcitons in CsPbBr Perovskite Nanocrystals Revealed by Femtosecond Transient-Absorption and Single-Dot Luminescence Spectroscopy

Naoki Yarita, Hirokazu Tahara, Toshiyuki Ihara, Tokuhisa Kawakami, Ryota Sato, Masaki Saruyama, Toshiharu Teranishi, and Yoshihiko Kanemitsu

*J. Phys. Chem. Lett.*, Just Accepted Manuscript • DOI: 10.1021/acs.jpclett.7b00326 • Publication Date (Web): 13 Mar 2017

Downloaded from <http://pubs.acs.org> on March 13, 2017

### Just Accepted

"Just Accepted" manuscripts have been peer-reviewed and accepted for publication. They are posted online prior to technical editing, formatting for publication and author proofing. The American Chemical Society provides "Just Accepted" as a free service to the research community to expedite the dissemination of scientific material as soon as possible after acceptance. "Just Accepted" manuscripts appear in full in PDF format accompanied by an HTML abstract. "Just Accepted" manuscripts have been fully peer reviewed, but should not be considered the official version of record. They are accessible to all readers and citable by the Digital Object Identifier (DOI®). "Just Accepted" is an optional service offered to authors. Therefore, the "Just Accepted" Web site may not include all articles that will be published in the journal. After a manuscript is technically edited and formatted, it will be removed from the "Just Accepted" Web site and published as an ASAP article. Note that technical editing may introduce minor changes to the manuscript text and/or graphics which could affect content, and all legal disclaimers and ethical guidelines that apply to the journal pertain. ACS cannot be held responsible for errors or consequences arising from the use of information contained in these "Just Accepted" manuscripts.



ACS Publications

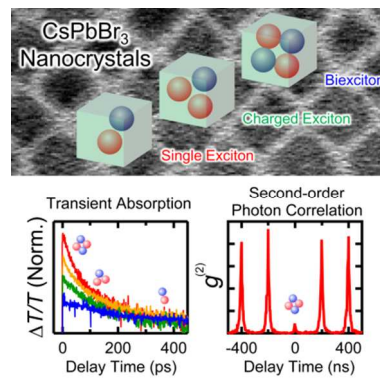
The Journal of Physical Chemistry Letters is published by the American Chemical Society. 1155 Sixteenth Street N.W., Washington, DC 20036

Published by American Chemical Society. Copyright © American Chemical Society. However, no copyright claim is made to original U.S. Government works, or works produced by employees of any Commonwealth realm Crown government in the course of their duties.

1  
2  
3  
4  
5  
6  
7 Dynamics of Charged Excitons and Biexcitons in  
8  
9  
10  
11 CsPbBr<sub>3</sub> Perovskite Nanocrystals Revealed by  
12  
13  
14  
15 Femtosecond Transient-Absorption and Single-Dot  
16  
17  
18  
19 Luminescence Spectroscopy  
20  
21  
22  
23  
24  
25  
26  
27  
28  
29  
30  
31  
32  
33  
34  
35  
36  
37  
38 AUTHOR INFORMATION  
39  
40  
41 Corresponding Author  
42  
43 \*kanemitu@scl.kyoto-u.ac.jp  
44  
45  
46  
47  
48  
49  
50  
51  
52  
53  
54  
55  
56  
57  
58  
59  
60

ABSTRACT: Metal-halide perovskite nanocrystals (NCs) are promising photonic materials for use in solar cells, light-emitting diodes, and lasers. The optoelectronic properties of these devices are determined by the excitons and exciton complexes confined in their NCs. In this study, we determined the relaxation dynamics of charged excitons and biexcitons in  $\text{CsPbBr}_3$  NCs using femtosecond transient-absorption (TA), time-resolved photoluminescence (PL), and single-dot second-order photon correlation spectroscopy. Decay times of  $\sim 40$  and  $\sim 200$  ps were obtained from the TA and PL decay curves for biexcitons and charged excitons, respectively, in NCs with an average size of 7.7 nm. The existence of charged excitons even under weak photoexcitation was confirmed by the second-order photon correlation function measurements. We found that charged excitons play a dominant role in luminescence processes of  $\text{CsPbBr}_3$  NCs. Combining different spectroscopic techniques enabled us to clarify the dynamical behaviors of excitons, charged excitons, and biexcitons.

## TOC GRAPHICS



Since the first reports on all solid-state perovskite solar cells were published in 2012,<sup>1,2</sup> lead halide perovskites have attracted enormous attention due to their optoelectronic properties. Recent studies of  $\text{CH}_3\text{NH}_3\text{PbI}_3$  and related perovskites have revealed their superior optical properties, such as sharp optical absorption edges and large absorption coefficients characteristic of direct-gap semiconductors,<sup>3–5</sup> the existence of nonexcitonic free carriers,<sup>6,7</sup> long carrier diffusion lengths,<sup>8–12</sup> photon recycling,<sup>13–16</sup> and high internal quantum efficiencies of photoluminescence (PL) at room temperature.<sup>17,18</sup> In addition to perovskite thin films and single crystals, perovskite nanocrystals (NCs) are also gathering attention as light-emitting materials. High-quality all-inorganic cesium lead halide perovskite ( $\text{CsPbX}_3$ , X = Cl, Br, I) NCs have been fabricated via colloidal synthesis methods<sup>19</sup> and exhibit unique optical properties, such as high PL quantum yields (QYs) of 50–90% and tunable bandgaps covering entire visible spectrum.<sup>19–21</sup> Efficient light-emitting diodes (LEDs)<sup>22</sup> and low-threshold lasing<sup>23,24</sup> have also been demonstrated recently.

In semiconductor NCs, optically or electronically generated electron–hole pairs are strongly correlated due to spatial confinement, leading to the formation of stable excitons. In the best-studied types of NCs, namely CdSe NCs and CdSe/ZnS, and CdSe/CdS core/shell NCs, unique optical processes appear due to the presence of excitons, trions (charged excitons), biexcitons, and multiple excitons.<sup>25–29</sup> Thus, it is crucial to thoroughly understand the behaviors of trions, biexcitons, and multiple excitons for the application of NCs in devices such as LEDs,<sup>30</sup> solar cells,<sup>31–35</sup> and single photon emitters.<sup>36,37</sup> The performances of these NC devices are strongly influenced by the nonradiative Auger recombination of trions, biexcitons, and multiple excitons in their NCs. In  $\text{CsPbX}_3$  perovskite NCs, three decay components were observed in femtosecond transient-absorption (TA) measurements, and their origins are under investigation.

<sup>38,39</sup> Moreover, the absorption cross-sections of CsPbX<sub>3</sub> NCs determined from TA measurements<sup>39</sup> are quite different from those obtained from single-dot luminescence spectroscopy.<sup>40</sup> From these standpoints, it is necessary to systematically measure the TA and PL dynamics in ensemble and single NC samples to clarify the origins of their decay time constants.

In this study, we investigated the dynamics of trions and biexcitons in CsPbBr<sub>3</sub> NCs using three different techniques: femtosecond TA, spectrally and time-resolved PL (TRPL), and single-dot second-order photon correlation  $g^{(2)}$  spectroscopy. We found that trions were efficiently photogenerated in the CsPbBr<sub>3</sub> NCs. Considering the trion contributions to the TA and TRPL signals, we were able to consistently explain the decay dynamics of exciton complexes and the absorption cross-section of NCs that were obtained via TA, TRPL, and single-dot PL spectroscopy. We also discuss the impact of trions on the optical properties of CsPbBr<sub>3</sub> NCs.

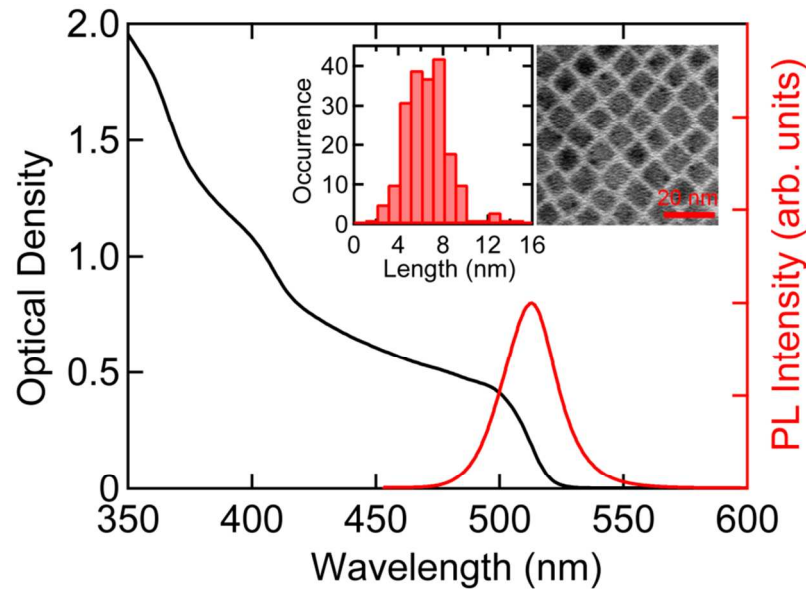


**Figure 1.** PL and absorption spectra of CsPbBr<sub>3</sub> NCs. The size distribution and a transmission electron microscope image are shown in the inset.

Figure 1 shows the PL and absorption spectra of  $\text{CsPbBr}_3$  NCs dispersed in hexane. Strong PL is observed at 512 nm, which corresponds closely to the lowest absorption edge. The inset displays a transmission electron microscope image of the sample and the size distribution of the cubic  $\text{CsPbBr}_3$  NCs with an average size of  $7.7 \pm 1.1$  nm.

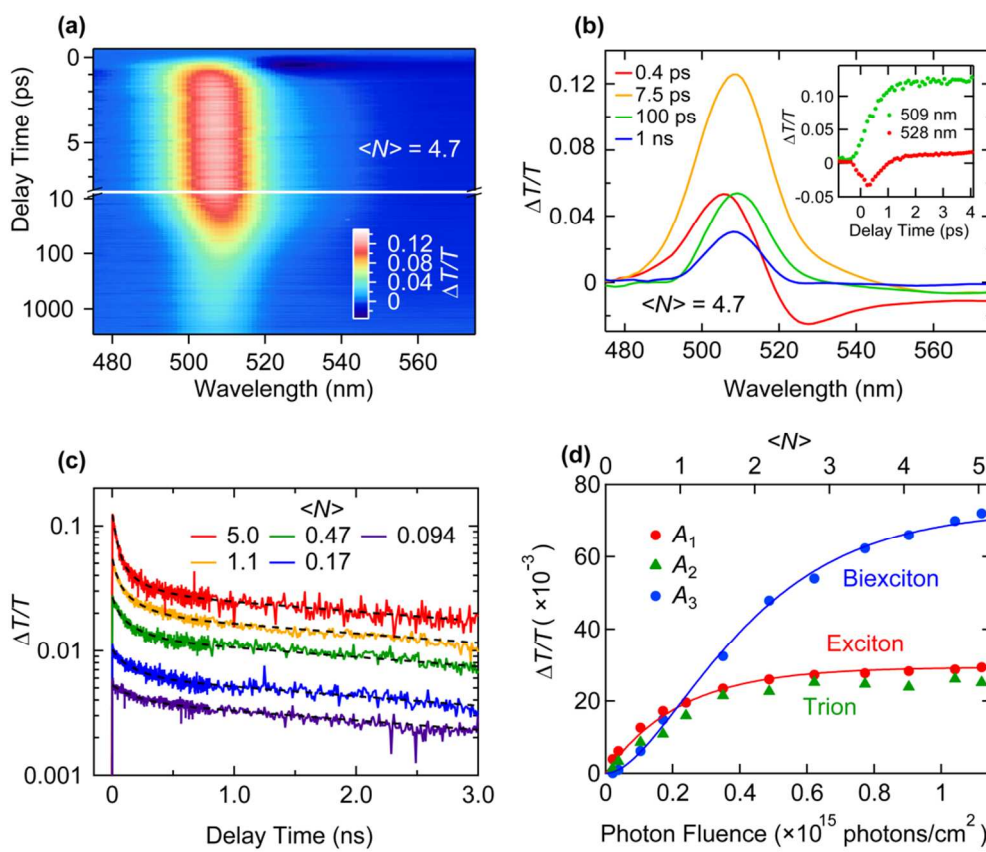


**Figure 2.** (a) Two-dimensional contour plot of TA spectra. (b) Time-dependent TA spectra at different delay times. The inset shows the temporal evolutions of the TA signals at 509 and 528 nm. (c) Dependence of the TA curves monitored at 509 nm on the excitation fluence. (d) Decay components  $A_1$ ,  $A_2$ , and  $A_3$  as functions of the excitation photon fluence.

Figure 2a shows a two-dimensional contour plot of the TA spectra of CsPbBr<sub>3</sub> NCs dispersed in hexane under continuous stirring to suppress the photocharging effect<sup>41</sup>, in which a photobleaching (PB) signal appears around 510 nm. For this experiment, the excitation wavelength was set to 400 nm. Detailed experimental methods for the femtosecond TA measurement are provided in the Supporting Information. Typical time-dependent TA spectra are illustrated in Figure 2b. Just after laser excitation, both PB and photoabsorption (PA) signals appear in the TA spectra. The shapes of these spectra are very similar to that of the second derivative of the linear absorption spectrum. The inset presents the temporal evolutions of the TA signals at 509 and 528 nm. The rise time of the 509 nm signal and the delay time at which the 528 nm signal appears are approximately determined by the duration of the excitation pulse. The spectral and dynamical behaviors around the zero delay time are determined by the cooling of photogenerated hot carriers.<sup>45</sup> The PA signals are caused by the transient Stark effect.<sup>42–45</sup> As the delay time increases, a strong PB signal appears at 509 nm and then it gradually decreases.

To analyze the relaxation process of the photogenerated carriers, we measured the dependence of the TA decay curves on the excitation fluence, as shown in Figure 2c. The average numbers of absorbed photons,  $\langle N \rangle$ , were determined from the excitation fluences (the evaluation procedure is described later). Note that  $\langle N \rangle = 1$  corresponds to a pulse energy density of 110  $\mu\text{J}/\text{cm}^2$  in this experiment. The TA dynamics were monitored at the strong PB peak (509 nm). Under weak excitation conditions ( $\langle N \rangle = 0.17$ ), the TA signal exhibits a single-exponential decay, indicating the relaxation dynamics of the single excitons. As the excitation laser fluence increases, two fast components clearly appear at delay times shorter than 500 ps. The TA decay curves can be fitted using triple exponential functions,  $A_1 e^{-t/\tau_1} + A_2 e^{-t/\tau_2} + A_3 e^{-t/\tau_3}$ . In the fitting procedure, we performed a global fitting for all decay curves,

where each excitation fluence has its own set of amplitudes but a single set of decay times was shared between the whole data. The single exciton decay time was set to  $\tau_1 = 5.7$  ns, which was determined based on the TRPL measurements (see Figure S1 in the Supporting Information). From this fitting analysis, we obtained the decay times of the two fast-decay components,  $\tau_2 = 190$  ps and  $\tau_3 = 39$  ps. These two components suggest that exciton complexes are generated under strong excitation.

To clarify the origins of the fast-decay components,  $A_2$  and  $A_3$ , the amplitudes of  $A_1$ ,  $A_2$ , and  $A_3$  are plotted in Figure 2d as a function of the excitation laser fluence. The dependence of  $A_2$  on the excitation fluence exhibits an increase similar to that of the single exciton amplitude ( $A_1$ ), while the fastest component ( $A_3$ ) increases more than  $A_1$  and  $A_2$ . To explain this behavior, we fitted the increasing functions with Poisson distributions. According to a Poisson distribution, the probability of exciton (biexciton) generation,  $P_X$  ( $P_{XX}$ ), is described as follows:

$$P_X(j_{\text{ex}}) = 1 - e^{-\sigma j_{\text{ex}}} \quad (1)$$

$$P_{XX}(j_{\text{ex}}) = 1 - e^{-\sigma j_{\text{ex}}} - \sigma j_{\text{ex}} e^{-\sigma j_{\text{ex}}} \quad (2)$$

where  $\sigma$  is the absorption cross-section of the  $\text{CsPbBr}_3$  NCs and  $j_{\text{ex}}$  is the excitation photon fluence. The average number of absorbed photons  $\langle N \rangle = \sigma j_{\text{ex}}$  can be determined from these values. Because the PB intensity due to excitons (biexcitons) is proportional to the number of excitons (biexcitons) generated in the NCs, the amplitudes of the different decay components can be expressed by these equations. The fits obtained using these equations (the red curve for excitons and the blue curve for biexcitons in Figure 2d) indicate that the  $A_1$  and  $A_3$  correspond closely to the saturation behaviors of  $P_X$  and  $P_{XX}$ , respectively. The obtained value of the absorption cross-section at 400 nm is  $4.5 \times 10^{-15} \text{ cm}^2$ , which is in good agreement with previously reported values for  $\text{CsPbBr}_3$  NCs of similar size.<sup>38,39</sup> These results clearly

demonstrate that the  $A_1$  and  $A_3$  components originate from excitons and biexcitons, respectively. On the other hand, we also analyzed the possibility of the existence of triexcitons by assigning the  $A_1$ ,  $A_2$ , and  $A_3$  components to excitons, biexcitons, and triexcitons, respectively. However, the calculated curves did not reproduce the experimental results (see Figure S2 in the Supporting Information). Therefore, we concluded that the  $A_2$  component is attributed to trions. The existence of trions even under stirring conditions indicates that they are more efficiently generated in  $\text{CsPbBr}_3$  NCs than in typical NCs, such as  $\text{CdSe}$  NCs.

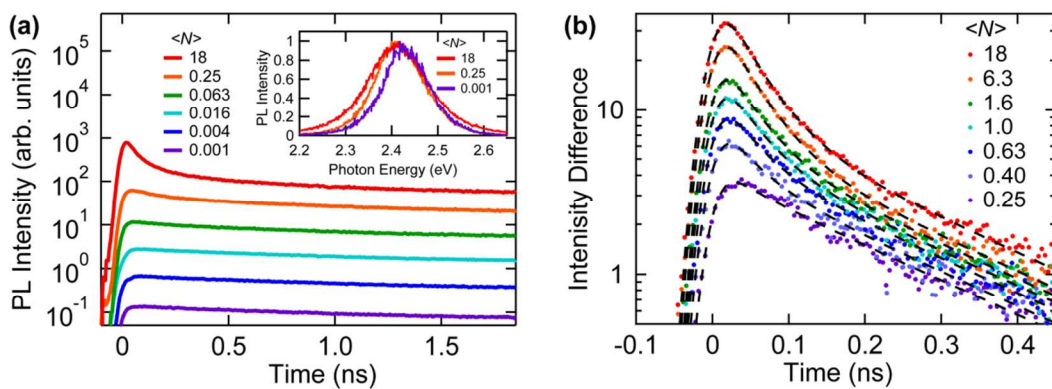


**Figure 3.** (a) Dependence of the PL decay curve of  $\text{CsPbBr}_3$  NCs on the excitation fluence. The inset shows the time-gated (0–100 ps) PL spectra at different excitation fluences. (b) Fast-decay components of the PL curves of  $\text{CsPbBr}_3$  NCs at different excitation fluences.

To confirm the existence of the two fast-decay components observed in the TA results, we performed TRPL measurements on  $\text{CsPbBr}_3$  NC ensembles. The used excitation wavelength was 430 nm and the time resolution of the TRPL measurements was  $\sim 40$  ps. Here,  $\langle N \rangle = 1$  corresponds to a pulse energy density of  $150 \mu\text{J}/\text{cm}^2$ . Figure 3a presents the resulting dependence of the PL decay curve on the excitation fluence. Under strong photoexcitations ( $\langle N \rangle \geq 0.25$ ), the fast-decay component appears, in addition to the slow-decay curve from the single excitons. The

1  
2  
3 inset shows the PL spectra of CsPbBr<sub>3</sub> NCs at early times (<100 ps) under different excitation  
4 fluences. The PL spectrum under weak excitation ( $\langle N \rangle = 0.001$ ) is symmetric, while the  
5 low-energy side of the PL spectrum increases under strong excitations ( $\langle N \rangle \geq 0.25$ ). This  
6 low-energy PL is observed only when the fast-decay component appears. This finding implies  
7 that the fast-decay, low-energy PL is caused by the radiative recombination of trions and  
8 biexcitons.  
9  
10

11 To determine the decay times of the fast components precisely, we subtracted the  
12 long-lifetime PL component from the PL decay curves. As mentioned above, the long-lifetime  
13 component due to single excitons was obtained from the decay curve at the lowest fluence,  
14  $\langle N \rangle = 0.001$  (also see Figure S1 in the Supporting Information). The results of this subtraction  
15 are presented in Figure 3b, which reveals that two fast components exist in the PL dynamics, as  
16 in the TA dynamics. The dashed curves in the figure represent fitting results using a  
17 double-exponential function convoluted with the detector response time, and we obtained the  
18 values 42 ps and 210 ps for the two decay times. The characteristics of the PL decay curves are  
19 highly consistent with those of the TA decay curves; thus, the 40-ps and 200-ps decay  
20 components originate from biexcitons and trions, respectively. This conclusion is also supported  
21 by the following theoretical consideration. In an ideal case, we are able to calculate the  
22 nonradiative Auger lifetimes of trion ( $\tau_{A,X^*}$ ) and biexciton ( $\tau_{A,XX}$ ) through the following two  
23 equations:<sup>46</sup>  $\tau_{A,X^*}^{-1} = \tau_{X^*}^{-1} - 2\tau_X^{-1}$  and  $\tau_{A,XX}^{-1} = \tau_{XX}^{-1} - 4\tau_X^{-1}$ , where  $\tau_X$ ,  $\tau_{X^*}$  and  $\tau_{XX}$   
24 represent the lifetimes of single exciton, trion, and biexciton, respectively. In the case that the  
25 positive and negative trions exhibit the same decay time  $\tau_{A,X^*}$ , both Auger lifetimes are related  
26 according to  $\tau_{A,X^*} = 4\tau_{A,XX}$ .<sup>46,47</sup> The experimentally evaluated ratios  $\tau_{A,X^*}/\tau_{A,XX}$  are obtained  
27  
28  
29  
30  
31  
32  
33  
34  
35  
36  
37  
38  
39  
40  
41  
42  
43  
44  
45  
46  
47  
48  
49  
50  
51  
52  
53  
54  
55  
56  
57  
58  
59  
60

to be  $\sim 5$  from TA and TRPL measurements, which is in good agreement with the ideal theoretical value 4.

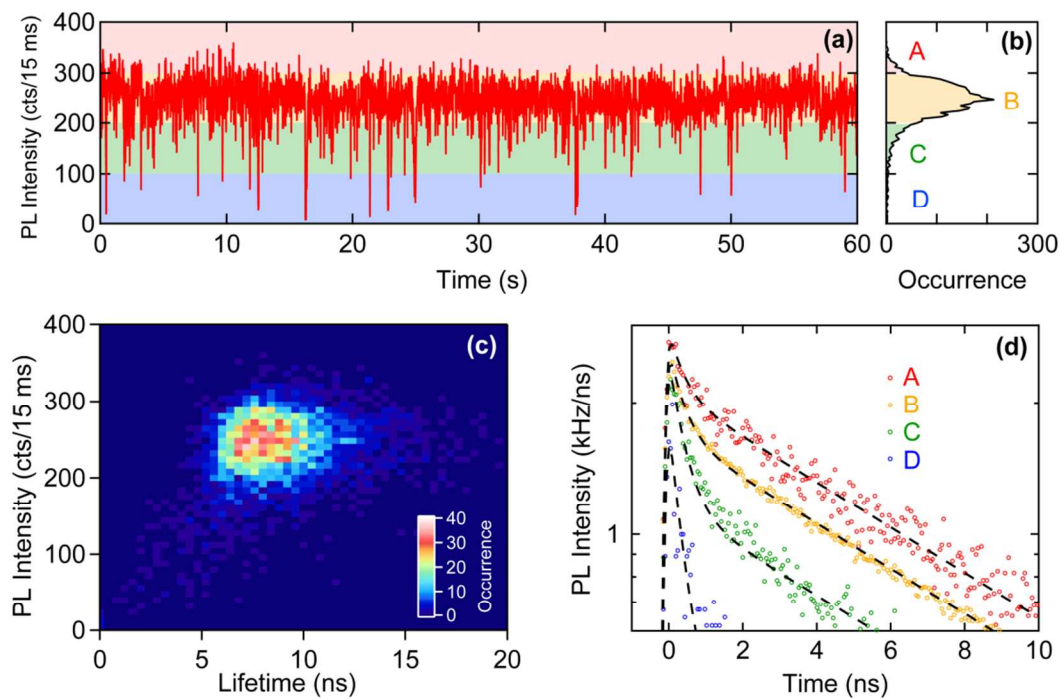


**Figure 4.** (a) PL intensity time trace under an excitation density of  $j_{\text{ex}} = 1.3 \mu\text{J}/\text{cm}^2$ , (b) PL intensity distribution, (c) Results of FLID analysis, and (d) TRPL decays derived from the data within the differently shaded areas in Figures 4a and 4b for the same single  $\text{CsPbBr}_3$  NC.

The abovementioned TA and TRPL measurements were carried out with NC ensemble samples. Furthermore, we measured the second-order photon correlations of single NC luminescence using single-dot PL techniques to analyze the exciton complexes. Figure 4a presents the time trace of the PL intensity of a single  $\text{CsPbBr}_3$  NC for an excitation wavelength of 430 nm. The fluctuation of the PL intensity is evident, and has also been observed in typical NCs, such as  $\text{CdSe/ZnS}^{26}$  and  $\text{CdSe/CdS}^{27}$  NCs. In these core/shell-type NCs, the PL intensity fluctuations are caused by fluctuations between the bright (on), intermediate (grey), and dark (off) states.<sup>26,27</sup> In contrast, the dark state (no light emission) is not observable for the single

CsPbBr<sub>3</sub> NCs, as is evident from Figure 4b. Figure 4c shows the correlation between PL lifetime and intensity, which is known as the fluorescence lifetime-intensity distribution (FLID). In Figure 4d, we provide the TRPL decay curves obtained by integrating the different-intensity parts denoted by A, B, C, and D in Figure 4b. The signals in the high-PL-intensity region (A) are dominantly determined by the long-lifetime single excitons. In contrast, the middle- and low-PL-intensity regions (B, C, and D) clearly exhibit fast-decay components. This double-exponential behavior strongly suggests that the observed PL dynamics are caused by the exciton and trion states. Based on the fitting by a double-exponential function convoluted with the detector response time, the lifetimes were determined to be 410 ps and 8.4 ns in this NC.

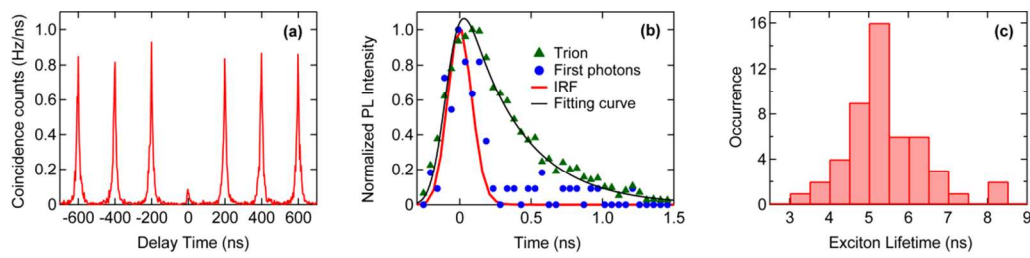


**Figure 5.** (a) Second-order correlation function  $g^{(2)}$  and (b) PL dynamics of trion and first photons. The red line is the instrument response function (IRF). (c) Distribution of the exciton lifetimes of single NCs.

The second-order photon correlation was also studied to analyze the one- and two-photon emission processes. Figure 5a shows the second-order photon correlation function  $g^{(2)}$ , where the ratio between the areas of the central and side peaks is 0.1. The central peak implies the two-photon emission process, i.e., the biexciton-exciton cascade emission.<sup>48</sup> The drop at the central peak means that the single NC almost always emits a single photon per one excitation pulse. Because the first (second) photon emission at the central peak in  $g^{(2)}$  is caused by the

transition from a biexciton to an exciton (from an exciton to the ground state), the first emitted photons can provide the biexciton decay curve.<sup>49–51</sup> Using this analysis and the time-tagged single-photon counting method, a TRPL signal was obtained from only the first photons and is shown in Figure 5b. The lifetime is shorter than the time resolution of our measurement system (~200 ps). This fast decay is consistent with the conclusion that the 40-ps decay components observed in the TA and PL experiments are due to biexciton recombination. Based on this result, we attributed the 410 ps decay component to triions, rather than to biexcitons.

Next, we investigated the exciton lifetimes of single NCs. Using single-dot spectroscopy, we determined the individual properties of perovskite NCs. The single exciton lifetime distribution is presented in Figure 5c. The broadness of the distribution suggests that the single exciton lifetimes are distributed similarly to the NC sizes shown in the inset of Figure 1. The average of the single exciton lifetimes measured using the 50 single NCs in this study is  $5.4 \pm 1.0$  ns, which is in good agreement with the value of 5.7 ns obtained from the NC ensemble TRPL results.

Single-dot spectroscopy also allowed us to estimate the absorption cross-sections  $\sigma$  of the individual NCs by using the following equation:<sup>52</sup>

$$\sigma = \frac{I_X}{F \cdot j_{\text{ex}} \cdot \eta_X \cdot \xi} \quad (4)$$

where  $I_X$  is the exciton PL count rate,  $F$  is the pump pulse repetition rate (5 MHz),  $\eta_X$  is the PL QY of the excitons, and  $\xi$  is the detection efficiency of our system. For CsPbBr<sub>3</sub> NCs,  $\eta_X$  has been reported to be 50–90%,<sup>19</sup> and  $\xi$  has been estimated to be 6–8%.<sup>52</sup> For an NC with a single exciton lifetime of 5.7 ns in Figure 5c,  $\sigma$  was calculated to be  $3–7 \times 10^{-15}$  cm<sup>2</sup> at 430 nm, which is comparable to the value determined from the ensemble TA results.

1  
2  
3 Note that the single exciton lifetimes of single NCs can be obtained even for NCs with  
4 relatively low PL intensities. In contrast, to obtain the  $g^{(2)}$  curve shown in Figure 5a, it was  
5 necessary to select the larger NCs within the size-distributed ensemble, because only these emit  
6 bright light. In fact, for the NC used to obtain the results shown in Figures 4, 5a, and 5b,  $\sigma$  was  
7 calculated to be  $1\text{--}4 \times 10^{-14}$  cm<sup>2</sup> at 430 nm, which is one order of magnitude greater than the  
8 cross-section resulting from the ensemble TA measurements. For this value of  $\sigma$ ,  $\langle N \rangle$  ranges  
9 from 0.04 to 0.1. Note that the PL dynamics of trions are prominent even under these  
10 low-excitation conditions, which is consistent with the efficient trion emission in the ensemble  
11 TRPL measurements (the inset of Fig. 3a).

12  
13  
14  
15  
16  
17  
18  
19  
20  
21  
22 In conclusion, we clarified the recombination dynamics of excitons, trions, and biexcitons  
23 in cubic CsPbBr<sub>3</sub> NCs using TA, TRPL, and single-dot spectroscopy. Combining the results  
24 obtained using these different spectroscopic techniques, we assigned the exciton, trion, and  
25 biexciton dynamics. Based on all the obtained data, we determined that the average lifetimes of  
26 biexcitons, trions, and single excitons are about 40 ps, 200 ps, and 6 ns, and that the absorption  
27 cross-section is  $4.5 \times 10^{-15}$  cm<sup>2</sup> at 400 nm for CsPbBr<sub>3</sub> NCs with an average size of 7.7 nm. We  
28 conclude that ionized states (trions) are formed more efficiently than neutral multiple excitons  
29 (triexcitons) in CsPbBr<sub>3</sub> perovskite NCs.

1  
2  
3 AUTHOR INFORMATION  
4  
56 Corresponding Author.  
7  
89 \*kanemitu@scl.kyoto-u.ac.jp  
10  
1112 Notes  
13  
1415 The authors declare no competing financial interests.  
16  
1718 ACKNOWLEDGMENT  
19  
2021 The authors thank T. Aharen, T. Yamada, T. Handa, and N. Hiroshige for helpful discussions  
22 and experimental help. Part of this work was supported by JST-CREST.  
23  
2425 ASSOCIATED CONTENT  
26  
2728  
29 **Supporting Information.** Sample preparation, details of femtosecond TA, TRPL, and single-dot  
30 second-order photon correlation  $g^{(2)}$  spectroscopy, PL decay curves, and the fitting analysis of  
31  
32 three decay components in TA decay curves. (PDF)  
33  
34  
3536 REFERENCES  
37  
38

- 39
- 
- 40 (1) Lee, M. M.; Teuscher, J.; Miyasaka, T.; Murakami, T. N; Snaith H. J. Efficient Hybrid Solar
- 
- 41 Cells Based on Meso-Superstructured Organometal Halide Perovskites.
- Science*
- 2012**
- , 338,
- 
- 42
- 
- 43 643–647.
- 
- 44
- 
- 45 (2) Kim, H.-S.; Lee, C.-R.; Im, J.-H.; Lee, K.-B.; Moehl, T.; Marchioro, A.; Moon, S.-J.;
- 
- 46 Humphry-Baker, R.; Yum, J.-H.; Moser, J. E.; et al. Lead Iodide Perovskite Sensitized
- 
- 47 All-solid-state Submicron Thin Film Mesoscopic Solar Cell with Efficiency Exceeding 9%.
- 
- 48
- 
- 49
- Sci. Rep.*
- 2012**
- , 2, 591.
- 
- 50
- 
- 51
- 
- 52
- 
- 53
- 
- 54
- 
- 55
- 
- 56
- 
- 57
- 
- 58
- 
- 59
- 
- 60

- (3) Yamada, Y.; Nakamura, T.; Endo, M.; Kanemitsu, Y. Near-Band-Edge Optical Responses of Solution-Processed Organic–inorganic Hybrid Perovskite  $\text{CH}_3\text{NH}_3\text{PbI}_3$  on Mesoporous  $\text{TiO}_2$  Electrodes. *Appl. Phys. Express* **2014**, *7*, 032302.
- (4) Wolf, S. D.; Holovsky, J.; Moon, S.-J.; Löper, P.; Niesen, B.; Ledinsky, M.; Haug, F.-J.; Yum, J.-H.; Ballif, C. Organometallic Halide Perovskites: Sharp Optical Absorption Edge and Its Relation to Photovoltaic Performance. *J. Phys. Chem. Lett.* **2014**, *5*, 1035–1039.
- (5) Shirayama, M.; Kadowaki, H.; Miyadera, T.; Sugita, T.; Tamakoshi, M.; Kato, M.; Fujiseki, T.; Murata, D.; Hara, S.; Murakami, T. N.; et al. Optical Transitions in Hybrid Perovskite Solar Cells: Ellipsometry, Density Functional Theory, and Quantum Efficiency Analyses for  $\text{CH}_3\text{NH}_3\text{PbI}_3$ . *Phys. Rev. Appl.* **2016**, *5*, 014012.
- (6) Yamada, Y.; Nakamura, T.; Endo, M.; Wakamiya, A.; Kanemitsu, Y. Photocarrier Recombination Dynamics in Perovskite  $\text{CH}_3\text{NH}_3\text{PbI}_3$  for Solar Cell Applications. *J. Am. Chem. Soc.* **2014**, *136*, 11610–11613.
- (7) Stranks, S. D.; Burlakov, V. M.; Leijtens, T.; Ball, J. M.; Goriely, A.; Snaith, H. J. Recombination Kinetics in Organic-Inorganic Perovskites: Excitons, Free Charge, and Subgap States. *Phys. Rev. Appl.* **2014**, *2*, 2034007.
- (8) Stranks, S. D.; Eperon, G. E.; Grancini, G.; Menelaou, C.; Alcocer, M. J. P.; Leijtens, T.; Herz, L. M.; Petrozza, A.; Snaith, H. J. Electron-Hole Diffusion Lengths Exceeding 1 Micrometer in an Organometal Trihalide Perovskite Absorber. *Science* **2013**, *342*, 341–344.
- (9) Xing, G.; Mathews, N.; Sun, S.; Lim, S. S.; Lam, Y. M.; Grätzel, M.; Mhaisalkar, S.; Sum, T. C. Long-range Balanced Electron- and Hole-transport Lengths in Organic-inorganic  $\text{CH}_3\text{NH}_3\text{PbI}_3$ . *Science* **2013**, *342*, 344–347.

- (10) Wehrenfennig, C.; Eperon, G. E.; Johnston, M. B.; Snaith, H. J.; Herz, L. M. High Charge Carrier Mobilities and Lifetimes in Organometal Trihalide Perovskites. *Adv. Mater.* **2014**, *26*, 1584–1589.
- (11) Dong, Q.; Fang, Y.; Shao, Y.; Mulligan, P.; Qiu, J.; Cao, L.; Huang, J. Electron-hole Diffusion Lengths > 175 μm in Solution-grown CH<sub>3</sub>NH<sub>3</sub>PbI<sub>3</sub> Single Crystals. *Science* **2015**, *347*, 967–970.
- (12) Shi, D.; Adinolfi, V.; Comin, R.; Yuan, M.; Alarousu, E.; Buin, A.; Chen, Y.; Hoogland, S.; Rothenberger, A.; Katsiev, K.; et al. Low Trap-state Density and Long Carrier Diffusion in Organolead Trihalide Perovskite Single Crystals. *Science* **2015**, *347*, 519–522.
- (13) Yamada, Y.; Yamada, T.; Le Phuong, P.; Maruyama, N.; Nishimura, H.; Wakamiya, A.; Murata, Y.; Kanemitsu, Y. Dynamic Optical Properties of CH<sub>3</sub>NH<sub>3</sub>PbI<sub>3</sub> Single Crystals as Revealed by One- and Two-photon Excited Photoluminescence Measurements. *J. Am. Chem. Soc.* **2015**, *137*, 10456–10459.
- (14) Yamada, T.; Yamada, Y.; Nishimura, H.; Nakaike, Y.; Wakamiya, A.; Murata, Y.; Kanemitsu, Y. Fast Free-Carrier Diffusion in CH<sub>3</sub>NH<sub>3</sub>PbBr<sub>3</sub> Single Crystals Revealed by Time-Resolved One- and Two-Photon Excitation Photoluminescence Spectroscopy. *Adv. Electron. Mater.* **2016**, *2*, 1500290.
- (15) Pazos-Outón, L. M.; Szumilo, M.; Lamboll, R.; Richter, J. M.; Crespo-Quesada, M.; Abdijalebi, M.; Beeson, H. J.; Vruini, M.; Alsari, M.; Snaith, H. J. Photon Recycling in Lead -Iodide Perovskite Solar Cells. *Science* **2016**, *351*, 1430–1433.
- (16) Yamada, T.; Yamada, Y.; Nakaike, Y.; Wakamiya, A.; Kanemitsu, Y. Photon Emission and Reabsorption Processes in CH<sub>3</sub>NH<sub>3</sub>PbBr<sub>3</sub> Single Crystals Revealed by Time-Resolved Two-Photon-Excitation Photoluminescence Microscopy. *Phys. Rev. Appl.* **2017**, *7*, 014001.

- (17) Wehrenfennig, C.; Liu, M.; Snaith, H. J.; Johnston, M. B.; Herz, L. M. Homogeneous Emission Line Broadening in the Organo Lead Halide Perovskite  $\text{CH}_3\text{NH}_3\text{PbI}_{3-x}\text{Cl}_x$ . *J. Phys. Chem. Lett.* **2014**, *5*, 1300–1306.
- (18) Ha, S.-T.; Shen, C.; Zhang, J.; Xiong, Q. Laser Cooling of Organic-Inorganic Lead Halide Perovskites. *Nat. Photonics* **2015**, *10*, 115–121.
- (19) Protesescu, L.; Yakunin, S.; Bodnarchuk, M. I.; Krieg, F.; Caputo, R.; Hendon, C. H.; Yang, R. X.; Walsh, A.; Kovalenko, M. V. Nanocrystals of Cesium Lead Halide Perovskites ( $\text{CsPbX}_3$ , X = Cl, Br, and I): Novel Optoelectronic Materials Showing Bright Emission with Wide Color Gamut. *Nano Lett.* **2015**, *15*, 3692–3696.
- (20) Nedelcu, G.; Protesescu, L.; Yakunin, S.; Bodnarchuk, M. I.; Grotevent, M. J.; Kovalenko, M. V. Fast Anion-Exchange in Highly Luminescent Nanocrystals of Cesium Lead Halide Perovskites ( $\text{CsPbX}_3$ , X = Cl, Br, I). *Nano Lett.* **2015**, *15*, 5635–5640.
- (21) Akkerman, Q. A.; D’Innocenzo, V.; Accornero, S.; Scarpellini, A.; Petrozza, A.; Prato, M.; Manna, L. Tuning the Optical Properties of Cesium Lead Halide Perovskite Nanocrystals by Anion Exchange Reactions. *J. Am. Chem. Soc.* **2015**, *137*, 10276–10281.
- (22) Li, X.; Wu, Y.; Zhang, S.; Cai, B.; Gu, Y.; Song, J.; Zeng, H.  $\text{CsPbX}_3$  Quantum Dots for Lighting and Displays: Room-Temperature Synthesis, Photoluminescence Superiorities, Underlying Origins and White Light-Emitting Diodes. *Adv. Funct. Mater.* **2016**, *26*, 2435–2445.
- (23) Yakunin, S.; Protesescu, L.; Krieg, F.; Bodnarchuk, M. I.; Nedelcu, G.; Humer, M.; Luca, G. D.; Fiebig, M.; Heiss, W.; Kovalenko, M. V. Low-Threshold Amplified Spontaneous Emission and Lasing from Colloidal Nanocrystals of Caesium Lead Halide Perovskites. *Nat. Commun.* **2015**, *6*, 8056.

- (24) Wang, Y.; Li, X.; Song, J.; Xiao, L.; Zeng, H.; Sun, H. All-Inorganic Colloidal Perovskite Quantum Dots: A New Class of Lasing Materials with Favorable Characteristics. *Adv. Mater.* **2015**, *27*, 7101–7108.
- (25) Klimov, V. I.; Mikhailovsky, A. A.; McBranch, D. W.; Leatherdale, C. A.; Bawendi, M. G. Quantization of Multiparticle Auger Rates in Semiconductor Quantum Dots. *Science* **2000**, *287*, 1011–1013.
- (26) Yoshikawa, N.; Hirori, H.; Watanabe, H.; Aoki, T.; Ihara, T.; Kusuda, R.; Wolpert, C.; Fujiwara, T. K.; Kusumi, A.; Kanemitsu, Y.; et al. Biexciton State Causes Photoluminescence Fluctuations in CdSe/ZnS Core/Shell Quantum Dots at High Photoexcitation Densities. *Phys. Rev. B* **2013**, *88*, 155440.
- (27) Spinicelli, P.; Buil, S.; Quélin, X.; Mahler, B.; Dubertret, B.; Hermier, J. -P. Bright and Grey States in CdSe-CdS Nanocrystals Exhibiting Strongly Reduced Blinking. *Phys. Rev. Lett.* **2009**, *102*, 136801.
- (28) Galland, C.; Ghosh, Y.; Steinbrück, A.; Sykora, M.; Hollingsworth, J. A.; Klimov, V. I.; Htoon, H. Two Types of Luminescence Blinking Revealed by Spectroelectrochemistry of Single Quantum Dots. *Nature* **2011**, *479*, 203–207.
- (29) Zhao, J.; Chen, O.; Strasfeld, D. B.; Bawendi, M. G. Biexciton Quantum Yield Heterogeneities in Single CdSe (CdS) Core (Shell) Nanocrystals and Its Correlation to Exciton Blinking. *Nano Lett.* **2012**, *12*, 4477–4483.
- (30) Shirasaki, Y.; Supran, G. J.; Bawendi, M. G.; Bulović, V. Emergence of Colloidal Quantum-Dot Light-Emitting Technologies. *Nat. Photonics* **2013**, *7*, 13–23.
- (31) Schaller, R. D.; Klimov, V. I. High Efficiency Carrier Multiplication in PbSe Nanocrystals: Implications for Solar Energy Conversion. *Phys. Rev. Lett.* **2004**, *92*, 186601.

- (32) Ellingson, R. J.; Beard, M. C.; Johnson, J. C.; Yu, P. R.; Micic, O. I.; Nozik, A. J.; Shabaev, A.; Efros, A. L. Highly Efficient Multiple Exciton Generation in Colloidal PbSe and PbS Quantum Dots. *Nano Lett.* **2005**, *5*, 865–871.
- (33) Ueda, A.; Matsuda, K.; Tayagaki, T.; Kanemitsu, Y. Carrier Multiplication in Carbon Nanotubes Studied by Femtosecond Pump-Probe Spectroscopy. *Appl. Phys. Lett.* **2008**, *92*, 233105.
- (34) Semonin, O. F.; Luther, J. M.; Choi, S.; Chen, H. Y.; Gao, J.; Nozik, A. J.; Beard, M. C. Peak External Photocurrent Quantum Efficiency Exceeding 100% via MEG in a Quantum Dot Solar Cell. *Science* **2011**, *334*, 1530–1533.
- (35) Hu, F.; Lv, B.; Yin, C.; Zhang, C.; Wang, X.; Lounis, B.; Xiao, M. Carrier Multiplication in a Single Semiconductor Nanocrystal. *Phys. Rev. Lett.* **2016**, *116*, 106404.
- (36) Fisher, B.; Caruge, J. M.; Zehnder, D.; Bawendi, M. Room-Temperature Ordered Photon Emission from Multiexciton States in Single CdSe Core-Shell Nanocrystals. *Phys. Rev. Lett.* **2005**, *94*, 087403.
- (37) Michler, P.; Imamoglu, A.; Mason, M. D.; Carson, P. J.; Strouse, G. F.; Buratto, S. K. Quantum Correlation among Photons from a Single Quantum Dot at Room Temperature. *Nature* **2000**, *406*, 968–970.
- (38) Makarov, N. S.; Guo, S.; Isaienko, O.; Liu, W.; Robel, I.; Klimov, V. I. Spectral and Dynamical Properties of Single Excitons, Biexcitons, and Trions in Cesium-Lead-Halide Perovskite Quantum Dots. *Nano Lett.* **2016**, *16*, 2349–2362.
- (39) Castañeda, J. A.; Nagamine, G.; Yassitepe, E.; Bonato, L. G.; Voznyy, O.; Hoogland, S.; Nogueira, A. F.; Sargent, E. H.; Cruz, C. H. B.; Padilha, L. A. Efficient Biexciton

1  
2  
3 Interaction in Perovskite Quantum Dots Under Weak and Strong Confinement. *ACS Nano*  
4  
5 **2016**, *10*, 8603–8609.  
6  
7

8 (40) Hu, F.; Zhang, H.; Sun, C.; Yin, C.; Lv, B.; Zhang, C.; Yu, W.; Wang, X.; Zhang, Y.; Xiao,  
9 M. Superior Optical Properties of Perovskite Nanocrystals as Single Photon Emitters. *ACS*  
10  
11 *Nano* **2015**, *9*, 12410–12416.  
12  
13  
14

15 (41) McGuire, J. A.; Joo, J.; Pietryga, J. M.; Schaller, R. D.; Klimov, V. I. New Aspects of Carrier  
16  
17 Multiplication in Semiconductor Nanocrystals. *Acc. Chem. Res.* **2008**, *41*, 1810–1819.  
18  
19

20 (42) Norris, D. J.; Sacra, A.; Murray, C. B.; Bawendi, M. G. Measurement of the Size Dependent  
21  
22 Hole Spectrum in CdSe Quantum Dots. *Phys. Rev. Lett.* **1994**, *72*, 2612–2615.  
23  
24

25 (43) Klimov, V. I.; Hunsche, S.; Kurz, H. Biexciton Effects in Femtosecond Nonlinear  
26  
27 Transmission of Semiconductor Quantum Dots. *Phys. Rev. B* **1994**, *50*, 8110–8113.  
28  
29

30 (44) Trinh, M. T.; Sfeir, M. Y.; Choi, J. J.; Owen, J. S.; Zhu, X.-Y. A Hot Electron–Hole Pair  
31  
32 Breaks the Symmetry of a Semiconductor Quantum Dot. *Nano Lett.* **2013**, *13*, 6091–6097.  
33  
34

35 (45) Okano, M.; Sakamoto, M.; Teranishi, T.; Kanemitsu, Y. Assessment of Hot-Carrier Effects  
36  
37 on Charge Separation in Type-II CdS/CdTe Heterostructured Nanorods. *J. Phys. Chem.*  
38  
39 *Lett.* **2014**, *5*, 2951–2956.  
40  
41

42 (46) Park, Y.-S.; Bae, W. K.; Pietryga, J. M.; Klimov, V. I. Auger Recombination of Biexcitons  
43  
44 and Negative and Positive Trions in Individual Quantum Dots. *ACS Nano* **2014**, *8*,  
45  
46 7288–7296.  
47  
48

49 (47) Vaxenburg, R.; Rodina, A.; Lifshitz, E.; Efros, A. L. Biexciton Auger Recombination in  
50  
51 CdSe/CdS Core/Shell Semiconductor Nanocrystals. *Nano Lett.* **2016**, *16*, 2503–2511.  
52  
53

54 (48) Nair, G.; Zhao, J.; Bawendi, M. G. Biexciton Quantum Yield of Single Semiconductor  
55  
56 Nanocrystals from Photon Statistics. *Nano Lett.* **2011**, *11*, 1136–1140.  
57  
58  
59  
60

- 1  
2  
3 (49) Park, Y.-S.; Bae, W. K.; Padilha, L. A.; Pietryga, J. M.; Klimov, V. I. Effect of the  
4 Core/Shell Interface on Auger Recombination Evaluated by Single-Quantum-Dot  
5 Spectroscopy. *Nano Lett.* **2014**, *14*, 396–402.  
6  
7 (50) Cannesson, D.; Biadala, L.; Buil, S.; Quélin, X.; Javaux, C.; Dubertret, B.; Hermier, J.-P.  
8 Blinking Suppression and Biexcitonic Emission in Thick-Shell CdSe/CdS Nanocrystals at  
9 Cryogenic Temperature. *Phys. Rev. B* **2014**, *89*, 035303.  
10  
11 (51) Ihara, T.; Biexciton Cascade Emission Reveals Absolute Absorption Cross Section of Single  
12 Semiconductor Nanocrystals. *Phys. Rev. B* **2016**, *93*, 235442.  
13  
14 (52) Ihara, T.; Kanemitsu, Y. Absorption Cross-section Spectrum of Single CdSe/ZnS  
15 Nanocrystals Revealed Through Photoluminescence Excitation Spectroscopy. *Phys. Rev. B*  
16 **2015**, *92*, 155311.  
17  
18  
19  
20  
21  
22  
23  
24  
25  
26  
27  
28  
29  
30  
31  
32  
33  
34  
35  
36  
37  
38  
39  
40  
41  
42  
43  
44  
45  
46  
47  
48  
49  
50  
51  
52  
53  
54  
55  
56  
57  
58  
59  
60

